Journal of Vibration and Acoustics. Received October 29, 2023;
Accepted manuscript posted June 11, 2024. doi:10.1115/1.4065752

Modelling and experiment of the vibro-acoustic response of cylindrical shells with internal substructures

Lei Zhang[a], Email: sleepearly959@gmail.com

Min Yu[a,b], Email: yumin@whut.edu.cn

Xianzhong Wang[a,b*], Email: xianzhongwang00@gmail.com

Mingfei Ba[a], Email: 767320579@qq.com

Zhaoming Pang[a] Email: pangzhaom@163.com

[a.]School of Naval Architecture, Ocean and Energy Power Engineering,

Wuhan University of Technology, Wuhan 430063, China

[b.]Key Laboratory of High Performance Ship Technology (Wuhan University of Technology), Ministry of Education, Wuhan 430063, China

Abstract

This study investigates the theoretical and experimental aspects of the vibro-acoustic characteristics of cylindrical shells with internal substructures. On the theoretical side, a hybrid calculation method is proposed, which combines the condensed transfer function method with the direct stiffness method and the precise transfer matrix method. The cylindrical shell with internal substructures is decoupled, and the governing equations for the cylindrical shell substructure and the internal substructure are separately established. Furthermore, the coupling forces between the cylindrical shell substructure and the plate substructure are solved based on the condensed transfer function method. These coupling forces are then incorporated into the overall transfer equation of the cylindrical shell to obtain the vibro-acoustic response of the coupled structure. Compared with the finite element calculation results, the validity of the calculation method in this paper is verified. In terms of experiments, the natural frequency, mode and vibration acoustic response of the model were tested, and compared with the theoretical results, which was in good agreement. The study demonstrates that the proposed hybrid calculation method based on the condensed transfer function is effective in predicting the vibro-acoustic characteristics of cylindrical shells with internal substructures.

Keywords

Internal substructures, cylindrical shells, vibro-acoustic characteristics, hybrid computational methods, experimental tests

1 Introduction

The coupled structure of a cylindrical shell with an internal substructure is extensively employed in practical engineering, often serving as a simplified model for submarines and other underwater vehicles. Therefore, researching the vibro-acoustic characteristics of such structures holds significant military value. Numerous domestic and international scholars have conducted studies on the acoustic and vibration characteristics of cylindrical shells and cylindrical shells with internal substructures. Leissa[1] and Qatu[2,3] have provided comprehensive summaries of relevant research on plates and shells. Peterson[4] analyzed the free vibration

*Corresponding author at: Xianzhong Wang, Key Laboratory of High Performance Ship Technology (Wuhan University of Technology), Ministry of Education, Wuhan 430063, China

E-mail address: xianzhongwang00@gmail.com

characteristics of a cylindrical shell with a longitudinal inner plate using the extended Rayleigh-Ritz method, obtaining natural frequencies and mode shapes of the coupled structure. Guo[5-7] expanded the investigation of acoustic characteristics to the internal coupling of cylindrical shells with a simple mass-spring system and explored the acoustic characteristics of rectangular plate shell structures. These studies have significantly bridged the gap between sound radiation theory research and practical engineering applications, highlighting the considerable impact of internal elements, such as simple mass-spring systems or rectangular plates, on the acoustic characteristics of cylindrical shells. Tso Y K[8] analyzed the transmission characteristics of vibration waves between semi-infinite cylindrical shells and plates using the wave method. Lee[9], based on the admittance method and Love thin shell theory, investigated the effects of shell length-diameter ratio, radius-thickness ratio, and fibre layer angle on the vibration characteristics of composite cylindrical shells incorporating rectangular plates. Smith and Haft[10] analyzed the natural vibration characteristics of a cylindrical shell enclosed by a circular plate at one end without considering the planar motion of the plate. Maxit and Ginoux[11] proposed a substructure method called CAA to predict the vibration and radiated noise of cylindrical shells with axisymmetric internal structures (ring ribs, bulkheads, end plates, etc.) underwater. Takahashi and Hirano[12] introduced a circular plate inside a cylindrical shell and analyzed its vibration characteristics. Huang[13] used the displacement admittance method to study the vibration of a boundary supported cylindrical shell with a circular baffle, in which the circular baffle can be located at any axial position. Missaoui J[14,15] developed an elastic connection model between slabs and cylindrical shells based on the Hamilton variational principle, primarily exploring the influence of connection stiffness on the free and forced vibration characteristics of the system. The direct stiffness method[16-18] uses the assembly strategy of the stiffness matrix in the classical finite element method to obtain the assembly of the overall stiffness matrix in an explicit way, which is used to solve the vibration of the plate with lateral or in-plane vibration. Wang[19-21] examined the acoustic characteristics of cylindrical shells, double-walled steel cylindrical shells, and conical-cylindrical shells using the precise transfer matrix method. Jiammeepreecha[22] used the membrane theory to analyze the nonlinear axisymmetric free vibration of a liquid-filled spherical shell with volume constraints. An analytical model was established by Zhang[23] to study the vibro-acoustic response of a double-layer cylindrical shell with a perforated inner wall under the excitation of pressure fluctuations in the external turbulent boundary layer. Gao[24] used the exact transfer matrix method to study the free vibration of a rubber-based cable-stiffened rotating composite shell under hydrostatic pressure. Meyer[25,26] proposed a condensed transfer function method based on the admittance method to analyze the vibration characteristics of non-axisymmetric structures inside cylindrical shells. Chen[27,28] proposed a unified analytical-numerical hybrid method for the coupled vibration analysis of stiffened hulls and non-axisymmetric internal structures. The vibro-acoustic characteristics of an underwater submarine shell with multiple internal substructures were studied by experiments and analysis. Jin[29] presented a unified vibration model for free vibration and forced vibration analysis of an open cylindrical shell-plate structure, and relevant simulation and experimental tests were carried out, but its sound radiation characteristics were not further considered. Su[30] studied the influence of non-axisymmetric substructures on the structure and acoustic characteristics of underwater ships, and established a fully coupled finite element / boundary element model of underwater ship structures. However, due to the limitations of the finite element / boundary element method, the analysis of the influence of substructures on the vibro-acoustic characteristics of underwater structures at high frequencies may not achieve satisfactory accuracy.

In this paper, a hybrid computational method based on the condensed transfer function method is adopted to solve the solution of the vibro-acoustic characteristics of a cylindrical shell with an internal substructure. The experimental research on related structures was carried out simultaneously. The core idea of this method is to use the direct stiffness method combined with the condensed transfer function method to obtain the vibration characteristics of a cylindrical shell with an internal substructure. First, the coupling force between the internal plate substructure and the cylindrical shell is extracted by matrix transformation, and then use the precise transfer

matrix method is used to calculate the sound radiation characteristics of the cylindrical shell with an internal substructure. The validity of the proposed method is verified by comparing the theoretical calculation results with the finite element calculation results. Finally, the validity and accuracy of the method are verified by comparing the results of the hybrid algorithm with the experimental test results, which can provide theoretical support for the prediction and evaluation of the vibro-acoustic characteristics of the cylindrical shell with internal substructure in practical engineering applications.

2. The Theoretical Model

The coupled structure, as shown in Fig 1, is decoupled into two substructures: the cylindrical shell substructure *a* and the internal plate substructure *b*. These two substructures are connected via coupling line 1 and coupling line 2. The control equations are established for each substructure, the line admittance matrix of the substructure *a* is obtained using the precise transfer matrix method, while the line admittance matrix of the substructure *b* is obtained using the direct stiffness method. Furthermore, the coupled forces between the substructure *a* and the substructure *b* are solved using the condensed transfer function method. These coupled forces are then incorporated into the overall transfer equation of the cylindrical shell substructure to obtain the vibro-acoustic response of the coupled structure.

Fig.1 Coupled Structure Schematic Diagram

2.1 Control Equation of substructure *a*

2.1.1 Overall Transfer Equation

The theoretical model of a cylindrical shell with internal substructures, as shown in Fig 1, is described as follows: where *h* represents the thickness of the cylindrical shell, and the thickness of the internal substructures is the same as that of the cylindrical shell. *L* denotes the length of the cylindrical shell, and *R* represents the radius. According to Flügge shell theory, when the cylindrical shell is subjected to excitation forces and sound pressure, the matrix differential equation for the structure can be expressed as:

$$\frac{\partial \mathbf{Z}(\xi)}{\partial \xi}=\mathbf{C}(\xi)\mathbf{Z}(\xi)+\mathbf{Q}(\xi) \tag{1}$$

where $\mathbf{Z}(\xi)=\left(\tilde{\mathrm{u}},\ \tilde{\mathrm{v}},\ \tilde{\mathrm{w}},\ \tilde{\phi},\ \tilde{\mathrm{M}}_X,\ \tilde{\mathrm{S}}_X,\ \tilde{\mathrm{V}}_X,\ \tilde{\mathrm{N}}_X\right)^{\mathrm{T}}$, where the elements represent the axial displacement, tangential displacement, radial displacement, twist angle, bending moment, radial shear force, tangential shear force, and axial shear force of the cylindrical shell. The elements in the matrix $\mathbf{C}(\xi)$ are detailed in Appendix A. and $\mathbf{Q}(\xi)$ represent the external force term due to concentrated forces and sound pressure. The general solution of Equation (1) is:

$$\mathbf{Z}(\xi)=\mathrm{e}^{\mathbf{C}\Delta\xi}\mathbf{Z}(\xi_0)+\int_0^{\xi}\mathrm{e}^{\mathbf{C}(\xi-\tau)}\mathbf{Q}(\tau)\mathrm{d}\tau \tag{2}$$

where $\mathbf{P}=\int_0^{\xi}\mathrm{e}^{[\mathbf{C}](\xi-\tau)}\mathbf{Q}(\tau)\mathrm{d}\tau$ represents the state response caused by the non-homogeneous term.

The transfer relationship between the state vectors $\mathbf{Z}(\xi)_L$ and $\mathbf{Z}(\xi)_R$ at the left and right ends of the cylindrical shell can be expressed as:

$$\mathbf{Z}(\xi)_R = \mathbf{T}\mathbf{Z}(\xi)_L + \mathbf{P} \tag{3}$$

where $\mathbf{T}=e^{[C]\Delta\xi}$ represents the field transfer matrix between the state vectors at the two ends.

For discretizing the cylindrical shell, a total of $n+1$ nodes are uniformly distributed, denoted as $1,2,\ldots,i,\ldots,n+1$, resulting in n segments. For the *i*-th segment, let the state vector at the left end be $\mathbf{Z}(\xi_i)$, and the state vector at the right end be $\mathbf{Z}(\xi_{i+1})$. Thus, the transfer relationship between the state vectors at both ends of this segment can be expressed using Equation (4):

$$-\mathbf{T}_{i+1}\mathbf{Z}(\xi_i) + \mathbf{Z}(\xi_{i+1}) = \mathbf{P}_{i+1} \tag{4}$$

By further assembling these segment transfer relationships, the overall transfer equation can be obtained as follows:

$$\begin{bmatrix} -\mathbf{T}_1 & \mathbf{I} & & & & \\ & -\mathbf{T}_2 & \mathbf{I} & & & \\ & & -\mathbf{T}_3 & \mathbf{I} & & \\ & & & \ddots & \ddots & \\ & & & & -\mathbf{T}_n & \mathbf{I} \end{bmatrix} \begin{bmatrix} \mathbf{Z}(\xi_1) \\ \mathbf{Z}(\xi_2) \\ \mathbf{Z}(\xi_3) \\ \vdots \\ \mathbf{Z}(\xi_n) \\ \mathbf{Z}(\xi_{n+1}) \end{bmatrix} = \begin{bmatrix} \mathbf{P}_1 \\ \mathbf{P}_2 \\ \mathbf{P}_3 \\ \vdots \\ \mathbf{P}_n \end{bmatrix} \tag{5}$$

2.1.2 Concentrated Forces

Assuming that the cylindrical shell is subjected to a concentrated force at a specific location (x_0,θ_0), this concentrated force can be represented using the Dirac delta function. By performing an orthogonal transformation calculation, the concentrated force can be expressed as:

$$f(x,\theta) = \delta(x-x_0)\sum_{\alpha=0}^{1}\sum_{n=0}^{\infty} f_n \sin\left(n\theta + \frac{\alpha\pi}{2}\right) \tag{6}$$

where:

$$f_n = \sum_{\alpha=0}^{1} f_0 \frac{\varepsilon_n}{2\pi}\sin\left(n\theta + \frac{\alpha\pi}{2}\right), \varepsilon_n = \begin{cases} 1, n=0 \\ 2, n\neq 0 \end{cases} \tag{7}$$

In the transfer matrix method, the application of a concentrated force will cause a change in the state vector of the specific segment of the cylindrical shell. Therefore, it is necessary to calculate the transfer matrix for each location where a concentrated force is applied. Assuming that a concentrated force acts at the position i, the relationship between the state vectors at the two ends of that position can be expressed as:

$$-\mathbf{Z}(\xi_i)_L + \mathbf{Z}(\xi_i)_R = \mathbf{F} \tag{8}$$

Based on equation (4), it can be observed that for the two segments of the cylindrical shell near the concentrated force, the relationship can be expressed as:

$$-\mathbf{T}\mathbf{Z}(\xi_{i-1}) + \mathbf{Z}(\xi_i^L) = \mathbf{P}_{i-1} \tag{9}$$

$$-\mathbf{T}\mathbf{Z}(\xi_i^R)+\mathbf{Z}(\xi_{i+1})=\mathbf{P}_i \tag{10}$$

Since the field transfer matrix $\mathbf{T}$ and the Duhamel integral term $\mathbf{P}$ can both be solved through integration, substituting equations (9) and (10) into equation (8) yields the state vectors at both ends of the concentrated force.

2.1.3 Sound Pressure

The acoustic pressure p in the fluid field needs to satisfy the Helmholtz equation, which can be expressed as:

$$\nabla^2 p+{k_0}^2 p=0 \tag{11}$$

where $k_0=\omega/c_0$, ω represents the circular frequency and c_0 represents the speed of sound in the fluid medium.

In an infinite ideal flow field, the acoustic pressure p needs to satisfy:

$$\lim_{r\to\infty}\sqrt{r}\left(\frac{\partial p}{\partial r}+ik_0 p\right)=0 \tag{12}$$

Assuming there are infinite rigid baffles at both ends of the cylindrical shell, the corresponding boundary conditions can be expressed as:

$$\left.\frac{\partial p}{\partial x}\right|_{x=0}=\left.\frac{\partial p}{\partial x}\right|_{x=l}=0 \tag{13}$$

By employing the method of separation of variables, the solution for the acoustic pressure in the fluid can be expressed as:

$$p=\sum_{n=0}^{\infty}\sum_{m=0}^{\infty}c_{mn}E_n\left(k_r r\right)\cos(k_m x)\sin(n\theta+\frac{\alpha\pi}{2}) \tag{14}$$

where c_{mn} represents the sound pressure coefficient when the axial wave number is n and the circumference wave number is m, and $k_m=m\pi/\mathrm{L}$, $m=0,1,2\ldots,k_r=\sqrt{k_0^2-k_m^2}$. α represents the symmetric mode when it is 1 and the anti-symmetric mode when it is 0. $E_n()$ varies with the change of k_r : if k_r is a real number, $E_n()$ corresponds to the second kind of Hankel function; if k_r is an imaginary number, $E_n()$ corresponds to the modified Neumann function.

2.1.4 Vibro-Acoustic Coupling Equation

In practical situations, the cylindrical shell is subjected to both concentrated forces and acoustic pressure. Based on the previous analysis, the state vectors of each discrete point can be separately obtained under the influence of concentrated forces and a certain order of generalized acoustic pressure. The combination of these two contributions yields the radial displacement at each node for a given order of radial wavenumber:

$$w(x)=\sum_{i=1}^{N}w_f\left(x_i\right)+\sum_{m=0}^{\infty}c_{mn}w_c\left(x\right) \tag{15}$$

where $w_c(x)$ represents the radial displacement response of the cylindrical shell under the generalized acoustic pressure of the (m,n) order, c_{mn} represents the acoustic pressure coefficient of the (m,n) order, and $w_f(x_i)$ represents the radial displacement response of the cylindrical shell at a discrete point i under the influence of concentrated forces. By superposing these responses, the radial displacement response of the cylindrical shell under the coupled force can be obtained. Hence, once the acoustic pressure coefficients are determined, the acoustic pressure in the flow field can be obtained using Equation (14). Therefore, the problem transforms into establishing equations for the acoustic pressure coefficients by considering other conditions in order to solve the acoustic pressure coefficients.

According to the continuity condition at the fluid-structure interface, at the interface between the shell and the external flow field, the radial velocity of the fluid is equal to the radial velocity of the shell:

$$\frac{1}{i\omega\rho}\frac{\partial p}{\partial r}=\frac{\partial w}{\partial t}\Big|_{r=R} \tag{16}$$

where ρ represents the density of the fluid.

By substituting equations (14) and (15) into equation (16), solving this equation will yield the values of the acoustic pressure coefficients.

$$\sum_{m=0}^{\infty} c_{mn}\left[\frac{dE_n(r)}{dr}\cos(k_m x_i)-\rho\omega^2 w_c\left(x_i\right)\right]=\rho\omega^2 w_f\left(x_i\right),(i=1,2,\ldots,M) \tag{17}$$

2.2 Control Equation of substructure *b*

This paper focuses on a cylindrical shell with an internal plate substructure. The plate is located inside the cylindrical shell at the middle position and connected to the cylindrical shell through coupling lines 1 and 2.

We can establish the vibration differential equation for the plate (substructure *b*) by employing the direct stiffness method.

$$\mathbf{M}_a\ddot{\mathbf{U}}_0^a+\mathbf{K}_a^*\mathbf{U}_0^a=\mathbf{F}_0^a \tag{18}$$

where $\mathbf{M}_a$、$\mathbf{K}_a^*=\mathbf{K}_a(1+j\eta_a)$ and $\mathbf{F}_0^a$ represent the mass matrix, complex stiffness matrix, and load vector of the substructure *b*, respectively. $\mathbf{U}_0^a$ represents the displacement amplitude of the substructure *b*.

When the angular frequency ω is determined, the steady-state displacement amplitude $\mathbf{U}_0^a$ of the structure can be computed, as shown in Equation (19).

$$\mathbf{U}_0^a=(-\omega^2\mathbf{M}_a+\mathbf{K}_a^*)^{-1}\mathbf{F}_0^a \tag{19}$$

2.3 The Treatment of Coupling

The gate function and the exponential function set naturally satisfy their mutually orthogonal mathematical properties and are relatively simple to express, so they are suitable as typical condensed functions. For the gate function, assuming that the length of the coupling line is L_s, the gate function can be defined as follows

$\varphi_n, n \in \{1,2,\cdots,N\}$:

$$\varphi_n(s) = \begin{cases} \dfrac{1}{\sqrt{L_s}} & (n-1) \le s \le nL_s \\ 0 & \text{other} \end{cases} \tag{20}$$

At this time, the number of condensed functions is N , and its inner product is defined as :

$$\langle f, g \rangle = \int_\Omega f(s) g^*(s) ds \tag{21}$$

The corner marker $*$ in means complex conjugate. Since the gate function is a piecewise continuous function set on the interval $[a,b]$, the gate function $\{\varphi_n\}_{1\le n\le N}$ has mutually orthogonal properties that can be easily verified, that is, the gate function belongs to the orthogonal set and meets the requirements of the condensed function.

In addition to the gate function, the exponential function set can also be used to describe the vibration wave at the structural coupling. The exponential function is shown as follows :

$$\varphi_n(s) = \frac{1}{\sqrt{L}} \exp\left(\frac{jn\pi s}{L}\right) \tag{22}$$

L : Coupling line length, j : Complex unit, $j^2 = 1$ 。According to the definition of inner product, there are also:

$$\langle f, g \rangle = \int_\Gamma f(s) g^*(s) ds \tag{23}$$

The calculation and verification show that the function set belongs to the orthogonal set and can also be used as a typical condensed function.

The control equations for the cylindrical shell and the internal substructure have been established in the previous context. The structure is coupled using the condensed transfer function method. According to the definition of the condensed transfer function method, for the uncoupled subsystem $\gamma(\gamma \in (a,b))$, the condensed transfer function between φ_n and φ_m, defined by applying force $\mathbf{F}_m^\gamma$ on the coupling line $\delta(\delta \in (1,2))$, is given by:

$$\mathbf{Y}_{nm}^\gamma = \left[\frac{\left\langle \bar{\mathbf{U}}_{m,q,p}^\gamma, \varphi_n \right\rangle}{\left\langle \left\langle \mathbf{F}_{m,q}^\gamma, \varphi_m \right\rangle \right\rangle} \right]_{1\le p\le 6, 1\le q\le 6} = \left[\left\langle \bar{\mathbf{U}}_{m,q,p}^\gamma, \varphi_n \right\rangle \right]_{p,q} \tag{24}$$

where $\langle \bullet, \bullet \rangle$ represents the inner product, φ_n represents the condensed function, $\mathbf{F}_m^\gamma$ represents the force applied on the coupling line, with components in each spatial direction represented by φ_m, p and q represent different spatial directions. The vector $\bar{\mathbf{U}}_{m,q}^\gamma$ represents the displacements of each node on the coupling line δ when the substructure is subjected to an excitation force $F_{m,q}^\gamma = \varphi_m$ in the q direction.

According to the definition of the condensed transfer function method, the coupling force $\mathbf{F}^{\gamma}$ and displacement $\mathbf{U}^{\gamma}$ at any position on the coupling line for each substructure can be expressed as a linear combination of condensed functions.

$$\begin{cases} \mathrm{F}^{\gamma}(s) \simeq \sum_{j=1}^{N} \mathrm{f}_j^{\gamma} \varphi_j(s) \\ \mathrm{U}^{\gamma}(s) \simeq \sum_{j=1}^{N} \mathrm{u}_j^{\gamma} \varphi_j(s) \end{cases} \tag{25}$$

where $\mathbf{f}_j^{\gamma}$ represents the force amplitude of substructure $\gamma(\gamma \in (a,b))$ associated with the condensed function φ_n, and $\mathbf{u}_j^{\gamma}$ represents the displacement amplitude of substructure γ associated with the condensed function φ_n.

When the coupling force, expressed using condensed functions, is applied to the corresponding structures, the steady-state displacements $\mathbf{U}_0^b$ of the cylindrical shell and $\mathbf{U}_0^a$ of the internal substructure can be separately obtained based on the control equations in Sections 2.1 and 2.2. Then, the admittance matrices $\mathbf{Y}^a$ and $\mathbf{Y}^b$ for the cylindrical shell and internal substructure can be determined.

Since the vibration control equation for the cylindrical shell is established in the cylindrical coordinate system $\{u, v, w, \phi_u, \phi_v, \phi_w\}^{\mathrm{T}}$, while the vibration control equation for the internal structure is established in the Cartesian coordinate system $\{u_x, u_y, u_z, \theta_x, \theta_y, \theta_z\}^{\mathrm{T}}$, a coordinate transformation matrix is required when coupling the cylindrical shell and the internal substructure. The relationship between the cylindrical coordinate system and the Cartesian coordinate system is given by:

$$\{u, v, w, \phi_u, \phi_v, \phi_w\}^{\mathrm{T}} = \mathbf{T}_b^{\mathrm{T}} \{u_x, u_y, u_z, \theta_x, \theta_y, \theta_z\}^{\mathrm{T}} \tag{26}$$

$$\mathbf{T}_b = \begin{bmatrix} 0 & -\sin\beta & \cos\beta & & & \\ 0 & \cos\beta & \sin\beta & & & \\ 1 & 0 & 0 & & & \\ & & & 0 & -\sin\beta & \cos\beta \\ & & & 0 & \cos\beta & \sin\beta \\ & & & 1 & 0 & 0 \end{bmatrix} \tag{27}$$

The free condensed displacement for substructure γ, which represents the displacement when substructure γ is subjected to external loads only, can be expressed as:

$$\tilde{\mathbf{u}}_j^{\gamma} = [\langle \tilde{\mathbf{U}}_p^{\gamma}, \varphi_j \rangle]_p \tag{28}$$

where $\tilde{\mathbf{U}}_p^{\gamma}$ represents the displacements at each node on the coupling line of substructure γ when substructure γ is subjected to external loads only, without any coupling effects.

According to the principle of linear superposition, the decoupled response of a substructure is the sum of the response under external excitation and the response under the effect of coupling forces. For substructure γ, we have on coupling line 1 and coupling line 2:

$$\mathbf{U}^{\gamma 0\delta} = \tilde{\mathbf{U}}^{\gamma 0\delta} + \sum_{j=1}^{N} \mathbf{U}_j^{\gamma 1\delta} \mathbf{f}_j^{\gamma 1} + \sum_{j=1}^{N} \mathbf{U}_j^{\gamma 2\delta} \mathbf{f}_j^{\gamma 2} \tag{29}$$

where $\mathbf{U}^{\gamma 0\delta}$ represents the displacement response of the nodes on the coupling line $\delta(\delta \in (1,2))$ in substructure $\gamma(\gamma \in (a,b))$ when subjected to external forces and the influence of the condensed transfer functions. $\tilde{\mathbf{U}}^{\gamma 0\delta}$ represents the free condensed displacement of the nodes on the coupling line δ in substructure γ when subjected to external forces only. $\mathbf{U}^{\gamma 1\delta}$ represents the displacement response of the nodes on the coupling line 1 in substructure γ when the condensed transfer functions force is applied on coupling line δ. $\mathbf{U}^{\gamma 2\delta}$ represents the displacement response of the nodes on the coupling line δ in substructure γ when the condensed transfer functions force is applied on coupling line 2. $\mathbf{f}_j^{\gamma 1}$ and $\mathbf{f}_j^{\gamma 2}$ represent the condensed transfer function forces applied on coupling line 1 and coupling line 2, respectively, in substructure γ.

According to the principle of linear superposition, the corresponding condensed displacement of substructure γ on the coupling line $\delta(\delta \in (1,2))$ can be obtained as follows:

$$\mathrm{u}_i^{\gamma 0\delta} = \tilde{\mathrm{u}}_i^{\gamma 0\delta} + \sum_{j=1}^{N} \mathrm{Y}_{ij}^{\gamma 1\delta} \mathrm{f}_j^{\gamma 1} + \sum_{j=1}^{N} \mathrm{Y}_{ij}^{\gamma 2\delta} \mathrm{f}_j^{\gamma 2} \tag{30}$$

where $\mathrm{Y}_{ij}^{\gamma 1\delta}$ represents the line admittance of the coupling line δ in substructure γ when the condensed transfer functions force is applied on coupling line 1. Similarly, $\mathrm{Y}_{ij}^{\gamma 2\delta}$ can be derived as the line admittance of the coupling line δ in substructure γ when the condensed transfer functions force is applied on coupling line 2.

Due to the continuity of displacement and force at the coupling line δ, the following conditions must be satisfied between substructure *b* (plate structure) and the substructure *a* (cylindrical shell structure):

$$\begin{cases} \mathrm{U}^{a0\delta} = \mathrm{U}^{b0\delta} \\ \mathrm{F}^{a\delta} = \mathrm{F}^{b\delta} \end{cases} \tag{31}$$

Due to the orthogonality of the functions, Equation (31) can be transformed into:

$$\begin{cases} \mathrm{u}^{a0\delta} = \mathrm{u}^{b0\delta} \\ \mathrm{f}^{a\delta} = \mathrm{f}^{b\delta} \end{cases} \tag{32}$$

By combining Equation (30) and Equation (32), we can write them in matrix form as follows:

$$\begin{bmatrix} \sum_{j=1}^{N}\mathbf{Y}_{ij}^{a11}+\sum_{j=1}^{N}\mathbf{Y}_{ij}^{b11} & \sum_{j=1}^{N}\mathbf{Y}_{ij}^{a21}+\sum_{j=1}^{N}\mathbf{Y}_{ij}^{b21} \\ \sum_{j=1}^{N}\mathbf{Y}_{ij}^{a12}+\sum_{j=1}^{N}\mathbf{Y}_{ij}^{b12} & \sum_{j=1}^{N}\mathbf{Y}_{ij}^{a22}+\sum_{j=1}^{N}\mathbf{Y}_{ij}^{b22} \end{bmatrix} \begin{Bmatrix} \mathbf{f}_j^{a1} \\ \mathbf{f}_j^{a2} \end{Bmatrix} = -\begin{Bmatrix} \tilde{\mathbf{u}}_i^{a01} \\ \tilde{\mathbf{u}}_i^{a01} \end{Bmatrix} \tag{33}$$

After a matrix transformation, Equation (33) can be represented as:

$$(\mathbf{Y}^a+\mathbf{Y}^b)\mathbf{F}=\tilde{\mathbf{U}}^{\mathrm{b}}-\tilde{\mathbf{U}}^{\mathrm{a}} \tag{34}$$

By simultaneously left-multiplying both sides of Equation (30) by $(\mathbf{Y}^a+\mathbf{Y}^b)^{-1}$, we can obtain the coupling forces on the coupling line 1 and coupling line 2 of the coupled structure. Substituting the coupling forces into Equation (5) will yield the vibro-acoustic characteristics of the coupled structure.

2.4 Verification

The coupling model shown in Fig.1 is established. The internal structure is a simplified plate, and the two long sides are rigidly connected to the cylindrical shell. Since the cylindrical shell and the internal plate are modeled in the same Cartesian coordinate system, the connection angle between the two can be ignored. The response of all nodes corresponds to six degrees of freedom. The parameters of cylindrical shell are: length l_c=1 m, radius r_c=0.3 m, thickness h_c=0.01 m; the structural parameters of the plate are: length l_p=1 m, width w_p=0.6 m, thickness h_p=0.01 m. The material parameters of different substructures are consistent: density ρ=7850 kg/m^3, structural loss factor η=0.01, elastic modulus E=210 Gpa, Poisson 's ratio μ=0.3. The excitation is the unit sinusoidal excitation force acting on the plate, and the direction is vertical downward along the axial direction. The position is (0,0,0.5), and the frequency range is 10~2000 Hz. The two ends of the cylindrical shell are simply supported, and the two ends of the plate are free. The condensed function is calculated by the gate function. It is verified that N takes 10 to meet the convergence requirements. The Fig 2 shows the radial mean square velocity of the cylindrical shell and the normal mean square velocity of the internal substructure obtained by this method and simulation. The Fig 3 shows the sound pressure level 1 m away from the axis center of the cylindrical shell. where lv represents the mean square vibration velocity level, and the unit is dB; SPL represents the sound pressure level, the unit is dB ; As can be seen from Figures 2 and 3, whether it is vibration response or sound response, the calculation results of the method in this paper and the finite element method are consistent. which can verify the reliability of the hybrid algorithm based on the condensed transfer function method in solving the vibration response problem of multi-coupled line structures.

Fig.2 Comparison and verification of mean square vibration velocity of coupled structure

Fig.3 Comparison and verification of sound pressure level of coupled structure

3. Experimental Test

3.1 Free Vibration Test

As shown in Fig 4(a), the modal testing system consists of a modal hammer, an accelerometer, a data acquisition device, and a computer. The experimental model is a cylindrical shell with an internal plate-like structure suspended by a crane, as depicted in Fig 4(b). Both the cylindrical shell and the inner plate are made of Q235 steel，The internal plate is fixed inside the cylindrical shell by welding. The dimensions of the cylindrical shell are as follows: length l_c=0.8 m, outer diameter r_c=0.265 m, and thickness h_c=0.008 m. The dimensions of the internal rectangular plate are as follows: length l_p=0.8 m, width w_p=0.514 m, and thickness h_p=0.008 m. A single-

point excitation and multiple-point response measurement method is employed for the modal experimental study. Before the modal test, the finite element software is used for modal calculation. According to the results of the finite element pre-analysis, the number of measuring points and the arrangement position are determined to ensure the reliability of the test results. The cylindrical shell is divided into 32 equal sections along the circumference and 8 equal sections along the axial direction. The internal plate-like substructure is divided into 8 equal sections along its length and 8 equal sections along its width. The acquired data is analyzed using a computer to obtain the natural frequencies of the model.

Fig.4 Modal experimental test

3.2 Forced Vibration Test

The testing system for forced vibration experiments is shown in Fig 5(a) and includes a signal generator, exciter, accelerometer, force sensor, data acquisition device, and computer. In the conducted study on forced vibration experiments, the cylindrical shell with the internal substructure is excited using the exciter, with the excitation point at the plate's center. The signal generator is set to a frequency range of 10-2000 Hz, with a frequency increment of 1 Hz/s. Since the structure is symmetrical, the following measurement points are selected as reference points, as shown in Fig 5(a).

A crane suspends the experimental model, and the exciter is fixed on a threaded rod. The threaded rod is connected to the end cap using bolts. The installation arrangement of the exciter is illustrated in Fig 5(b). The acquired data is analyzed using a computer to obtain the acceleration frequency response curves for each measurement point.

Fig.5 Forced vibration experimental test

3.3 Sound Radiation Test

The underwater sound radiation experimental testing system is shown in Fig 6(a) and includes a signal generator, exciter, force sensor, power amplifier, hydrophone, data acquisition device, and computer. The anechoic tank used in the test is 8 meters long, 4 meters wide, and 3.5 meters deep. There are high-precision multi-directional driving and lifting devices above the tank. The pool body is a straight-wall reinforced concrete structure. Conical rubber sound absorption wedges are laid in six directions on the inner wall, evenly arranged on six sides of the pool, and the sound waves incident on the surface are almost completely absorbed, thus simulating the infinite flow field of the ocean. In the experimental study of underwater sound radiation, the exciter is used to excite the cylindrical shell with internal substructures. The excitation point is located at the center of the plate. The signal generator is set within the frequency range of 10-2000 Hz, with a frequency increment of 1 Hz/s. The hydrophone is positioned as depicted in Fig 6(a). The experimental setup and the installation method of the hydrophone are shown in Fig 6(b) and Fig 6(c), respectively. The acquired data is analyzed using a computer to obtain the sound pressure level curves for each measurement point.

Fig.6 Experimental test of underwater sound radiation

4. Results and Discussions

4.1 Free Vibration

Based on the finite element method, a numerical model of the coupled structure is developed. To ensure sufficient accuracy in the structural discretization, an appropriate mesh size is selected based on the calculated frequency limits. The natural frequencies of the coupled structure are then computed. The results of the comparison between the finite element results and experimental results are presented in Table 1.

Table. 1 Comparison of natural frequency

From Table 1, it can be observed that the measured results of the natural frequencies for the coupled model are in good agreement with the numerical results, with the exception of the fourth mode, where the error exceeds 5%, indicating that the precision requirements for model fabrication in the experiments have been met and the experimental procedure is correct. This confirms that subsequent experimental tests and calculations can be conducted successfully.

4.2 Forced Vibration

Fig 7 presents a comparison between the measured and theoretical values of the vibration response for the coupled model. The experimental values represent the magnitudes of acceleration obtained at various measurement points using a data acquisition device. These values are then converted into acceleration levels at each point based on the reference points of the coupled structure. The theoretical values are obtained through the hybrid computational method proposed in this paper.

From Fig 7, it can be observed that there is a significant discrepancy between the experimental and theoretical values in the frequency range of 10-100 Hz. This discrepancy can be attributed to the fact that the boundary conditions used to simulate the end caps, which are modelled as simply supported, are not entirely equivalent. In the frequency range of 100-500 Hz, the vibration acceleration levels of the coupled model exhibit distinct peaks, and the frequencies and magnitudes of these peaks at different measurement points are in good agreement with the theoretical values. This indicates that the inherent vibration characteristics of the coupled model can be reflected accurately. In the frequency range of 500-1000 Hz, the experimental results show more peaks and higher amplitudes compared to the theoretical solutions. This is attributed to the presence of local vibrations caused by welding defects during the fabrication of the model, resulting in an increase in local modes and amplification of vibration amplitudes. In the frequency range of 1000-2000 Hz, the discrepancy between the experimental and theoretical values increases, which can be attributed to signal distortion in the exciter at high frequencies.

Fig.7 The vibration response of the reference point

Fig 8 presents a comparison of the average vibration response for the coupled structure. Overall, within the target frequency range of 10-2000 Hz, both the average vibration response and the vibration response at individual reference points obtained from the hybrid algorithm proposed in this paper show a good fit with the experimental test results in terms of the curve trends and magnitude. This indicates that the hybrid computational method proposed in this paper has sufficient accuracy and applicability in calculating the vibration response of cylindrical shells with internal substructures. It demonstrates the capability to address practical problems effectively.

Fig.8 Mean vibration response of coupled structures

4.3 Sound Radiation

Fig.9 is the comparison chart between the measured value and the theoretical value of the sound radiation response of the coupling model. The experimental value is obtained by the data acquisition instrument, and the sound pressure of each reference point of the coupling structure is transformed into the sound pressure level of the point. The theoretical value is the calculation result obtained by the hybrid calculation method.

Fig.9 Sound pressure at the reference point

From the curves in Fig 9(a) and Fig 9(b), it can be observed that below 1000 Hz, the computational results from the method proposed in this paper show good agreement with the experimental values. However, as the frequency increases, the discrepancy between the computational and experimental values becomes larger. On the one hand, due to the limitation of experimental environment and conditions, the vibrator used is easy to cause signal distortion at high frequency. In addition, the cut-off frequency of the anechoic tank is 2000 Hz, which means that the acoustic reflection in the tank cannot be ignored in the measurement frequency range, but its influence is

obvious at very low frequency and decreases with the increase of frequency. This experiment is still reliable in the measurement frequency range. This is consistent with the findings from the vibration response calculations.

In general, it can be seen that the curve of the experimental test results shows a significant left shift, indicating that the natural frequency of the structure is reduced. This is because the hybrid algorithm in this paper considers the influence of acoustic pressure on the structure in the fluid when solving the acoustic radiation, and ignores the fluid effect when solving the coupling force. The presence of fluid will increase the additional mass of the structure, resulting in a decrease in the natural frequency.

Additionally, in the method proposed in this paper, it is assumed that there are infinite baffles at both ends of the cylindrical shell. Therefore, when the hydrophone is placed outside the axial length of the shell, there should be significant deviations in the calculated sound pressure. This is also reflected in Fig 9(c), corresponding to the third hydrophone position.

5 Conclusions

The present study employs a hybrid computational approach combining condensed transfer function, precise transfer matrix method, and direct stiffness method to investigate the vibro-acoustic characteristics of cylindrical shells with internal substructures. Experimental results are compared with theoretical values, leading to the following conclusions:

(1) The modal test results exhibit good agreement with finite element analysis in terms of natural frequencies, indicating the adequacy of the experimental procedure and methodology in meeting accuracy requirements.

(2) For the coupled vibration response of the structure in air, significant peaks in vibration acceleration levels are observed for the cylindrical shell model with internal substructures at lower frequencies, with close alignment between the experimental and theoretical vibration response curves. However, at higher frequencies, additional local modes are present due to manufacturing processes, distortions in the excitation signal, and the fitting of the acceleration sensors to the structure, leading to deviations between experimental and theoretical vibration response curves.

(3) Regarding the sound radiation response of the coupled structure in water, the introduced method considers the influence of acoustic fluid pressure on the coupled structure only during the calculation of sound radiation characteristics while neglecting fluid effects in the calculation of coupled forces. As a result, the experimental frequency response curves show a noticeable leftward shift.

(4) In the target frequency range, the proposed hybrid computational approach based on condensed transfer functions demonstrates good consistency with experimental results, confirming its accuracy and reliability for analyzing the vibro-acoustic characteristics of cylindrical shells with internal substructures.

Acknowledgements

Our work is financially supported by the National Natural Science Foundation of China (No. 52271291).

Appendix A

$$\lambda^2 = \frac{\rho h R^2 \omega^2}{D}$$

$$C_{12} = -\mu n,\ \ C_{13} = -\mu,\ \ C_{18} = \frac{\tilde{h}}{12},\ \ C_{21} = n,\ \ C_{24} = \frac{n\tilde{h}^2}{6},\ \ C_{27} = \frac{\tilde{h}}{6(1-\mu)}$$

$$C_{34} = 1,\ \ C_{43} = \mu n^2,\ \ C_{45} = \frac{1}{\tilde{h}},\ \ C_{54} = 2(1-\mu)n^2\tilde{h},\ \ C_{56} = 1$$

$$C_{62}=\frac{12\left(1-\mu^2\right)n}{\tilde{h}},\quad C_{63}=\frac{12\left(\lambda^2+\mu^2-1\right)}{\tilde{h}}-\left(1-\mu^2\right)n^4\tilde{h},\quad C_{65}=\mu n^2,\quad C_{68}=-\mu$$

$$C_{72}=\frac{12\left(1-\mu^2\right)n^2}{\tilde{h}}-\frac{12\lambda^2}{\tilde{h}},\quad C_{73}=\frac{12\left(1-\mu^2\right)n}{\tilde{h}}+\left(1-\mu^2\right)n^3\tilde{h},\quad C_{75}=-\mu n,\quad C_{78}=\mu n$$

$$C_{81}=-\frac{12}{\tilde{h}}\lambda^2,\quad C_{84}=\left(1-\mu\right)n^2\tilde{h},\quad C_{87}=-n$$

References

[1] Leissa A W, Nordgren R P. Vibration of Shells[J]. Journal of Applied Mechanics, 1993, 41(2):544.

[2] Qatu M S. Recent research advances in the dynamic behavior of shells: 1989-2000, Part 1: Laminated composite shells[J]. Applied Mechanics Review, 2002, 55:325-350.

[3] Qatu M S. Recent research advances in the dynamic behavior of shells: 1989-2000, Part 2: Homogeneous shells[J]. Applied Mechanics Reviews, 2002:415-434.

[4] Peterson M R, DE Boyd. Free vibrations of circular cylinders with longitudinal interior partitions[J]. Journal of Sound and Vibration, 1978, 60(1):45-62.

[5] Guo, Y. P. Acoustic scattering from cylindrical shells with deck‐type internal plate at oblique incidence[J]. Journal of the Acoustical Society of America, 1996, 99(5):2701-2713.

[6] Guo Y. P. Sound scattering from an internally loaded cylindrical shell[J]. Journal of the Acoustical Society of America, 1992, 91(2):926-938.

[7] Guo Y.P. Sound scattering by bulkheads in cylindrical shells[J]. Journal of the Acoustical Society of America, 1994, 95(5):2550-2559.

[8] Tso Y K, Hansen C H. Wave propagation through cylinder/plate junctions[J]. Journal of Sound and Vibration, 1995, 186(3):447-461.

[9] Lee Y S, Choi M H, Kim J H. Free vibrations of laminated composite cylindrical shells with an interior rectangular plate[J]. Journal of Sound and Vibration, 2003, 265(4):795-817.

[10] Haft E E, Smith B L. Vibration of a circular cylindrical shell closed by an elastic plate.[J]. Aiaa Journal, 2012, 5(11):2080-2082.

[11] Maxit L, Ginoux J M. Prediction of the vibro-acoustic behavior of a submerged shell non periodically stiffened by internal frames[J]. Journal of the Acoustical Society of America, 2010, 128(1):137-151.

[12] Takahashi S, Hirano Y. Vibration of a Combination of Circular Plates and Cylindrical Shells: 1st Report, A Cylindrical Shell with Circular Plates at Ends[J]. Bulletin of Jsme, 2008, 35(274):1215-1222.

[13] Huang D T, Soedel W. Study of the Forced Vibration of Shell-Plate Combinations Using the Receptance Method[J]. Journal of Sound and Vibration, 1993, 166(2):341-369.

[14] Missaoui J, Cheng L. Vibroacoustic analysis of a finite cylindrical shell with internal floor partition[J]. Journal of Sound and Vibration,1999,226(1):101-123.

[15] Missaoui J, Cheng L, Richard M J . Free and forced vibration of a cylindrical shell with a floor partition[J]. Journal of Sound and Vibration,1996,190(1):21-40.

[16] Danial A N, Doyle J F. Dynamic analysis of folded plate structures on a massively parallel computer[J]. Computers and Structures, 1995, 54(3):521-529.

[17] Casimir J B, Kevorkian S, Vinh T. The dynamic stiffness matrix of two-dimensional elements: application to Kirchhoff\"s plate continuous elements[J]. Journal of Sound and Vibration, 2005, 287(3):571-589.

[18] Li H, Yin X, Wu W. Dynamic stiffness formulation for in-plane and bending vibrations of plates with two opposite edges simply supported[J]. Journal of Vibration and Control. 2016，24(9): 1652-1669.

[19] Wang X, Chen D, Xiong Y,Jiang Q, Zuo Y. Experiment and modeling of vibro-acoustic response of a

stiffened submerged cylindrical shell with force and acoustic excitation[J]. Results in Physics,2018,11:315-324.

[20] Wang X, Jiang Q, Xiong Y, Gu X. Experimental studies on the vibro-acoustic behavior of a stiffened submerged conical-cylindrical shell subjected to force and acoustic excitation[J]. Journal of Low Frequency Noise, Vibration and Active Control, 2020, 39(2): 280-296.

[21] Wang X, Chen L, Li N, Xia Y, Xiong Y. An Experimental and Modeling Study on Vibro-Acoustic Response of Double-Walled Steel Cylindrical Shells[J]. International Journal of Steel Structures, 2020, 20(4):1081-1099

[22] Jiammeepreecha W, Chucheepsakul S. Nonlinear axisymmetric free vibration analysis of liquid-filled spherical shell with volume constraint[J]. Journal of Vibration and Acoustics, 2017, 139(5): 051016.

[23] Zhang Q, Mao Y, Qi D. Analytical modeling of the vibro-acoustic response of a double-walled cylindrical shell with microperforation excited by turbulent boundary layer pressure fluctuations[J]. Journal of Vibration and Acoustics, 2018, 140(2): 021012.

[24] Gao H, Shuai C, Ma J, Xu G. Free vibration of rubber matrix cord-reinforced combined shells of revolution under hydrostatic pressure[J]. Journal of Vibration and Acoustics, 2022, 144(1): 011002.

[25] Meyer V, Maxit L, Guyader J L, Leissing T, Audoly C. A condensed transfer function method as a tool for solving vibroacoustic problems[J]. Proceedings of the Institution of Mechanical Engineers, Part C: Journal of Mechanical Engineering Science, 2015:928-938.

[26] Meyer V, Maxit L, Guyader J L, Leissing T. Prediction of the vibroacoustic behavior of a submerged shell with non-axisymmetric internal substructures by a condensed transfer function method[J]. Journal of Sound and Vibration, 2016, 360:260-276.

[27] Jia W, Chen M, Xie K, Dong W. Experimental and analytical investigations on vibro-acoustic characteristics of a submerged submarine hull coupled with multiple inner substructures[J]. Ocean Engineering, 2022, 259: 111960.

[28] Jia W, Chen M, Xie K, Zhou Z. Theoretical and experimental studies of effects of non-axisymmetric inner structures on vibration signatures of axisymmetric submarine hulls[J]. Applied Mathematical Modelling, 2023, 120: 485-512.

[29] Li Z, Jin G, Ye T, Tang T, Zhong S, Tian L. A unified vibration modeling of open cylindrical shell-rectangular plate coupling structures based on the dynamic stiffness method[J]. Journal of Sound and Vibration, 2023: 117870.

[30] Su J, Lei Z, Qu Y, Hua H. Effects of non-axisymmetric structures on vibro-acoustic signatures of a submerged vessel subject to propeller forces[J]. Applied Acoustics, 2018, 133: 28-37.

Figure Captions List

Journal of Vibration and Acoustics. Received October 29, 2023;
Accepted manuscript posted June 11, 2024. doi:10.1115/1.4065752

Table Captions List

Journal of Vibration and Acoustics. Received October 29, 2023;
Accepted manuscript posted June 11, 2024. doi:10.1115/1.4065752

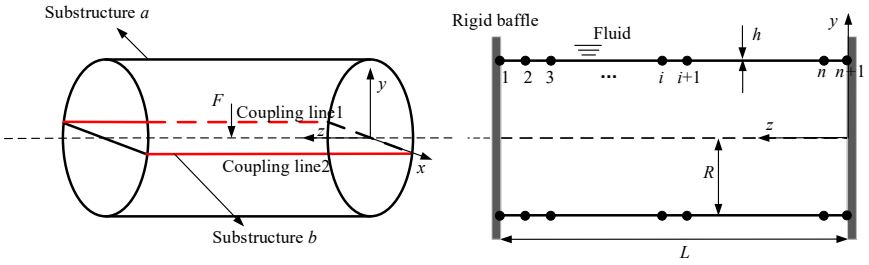

Fig.1 Coupled Structure Schematic Diagram

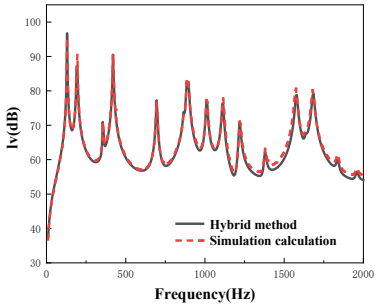

(a) Normal mean square vibration velocity of flat plate

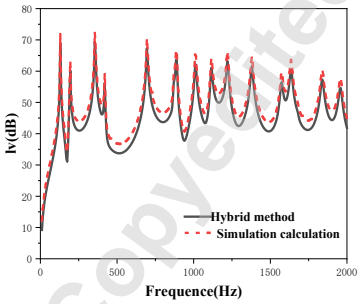

(b) Radial mean square vibration velocity of cylindrical shell

Fig.2 Comparison and verification of mean square vibration velocity of coupled structure

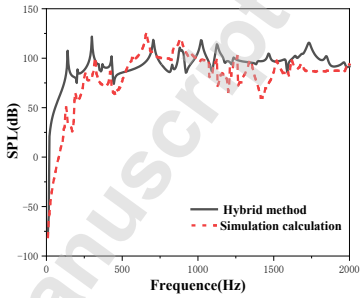

Fig.3 Comparison and verification of sound pressure level of coupled structure

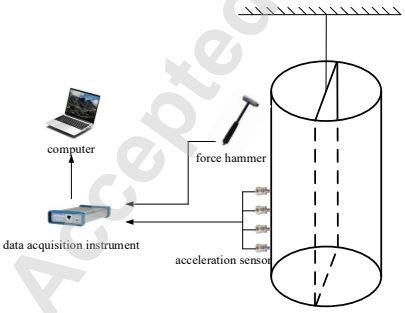

(a) Experimental system

(b) Experimental set-up

Fig.4 Modal experimental test

Journal of Vibration and Acoustics. Received October 29, 2023;
Accepted manuscript posted June 11, 2024. doi:10.1115/1.4065752

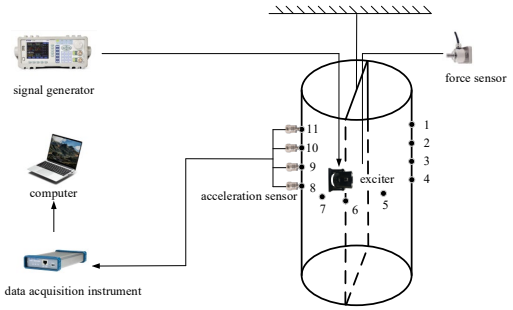

(a) Experimental test system

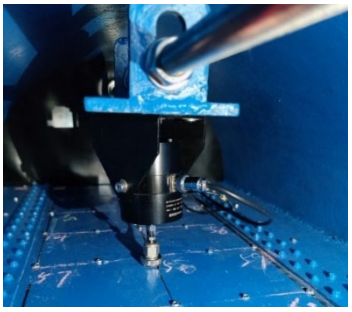

(b) Installation of exciter

Fig.5 Forced vibration experimental test

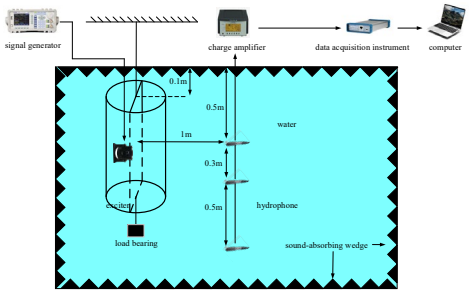

(a) Experimental test system

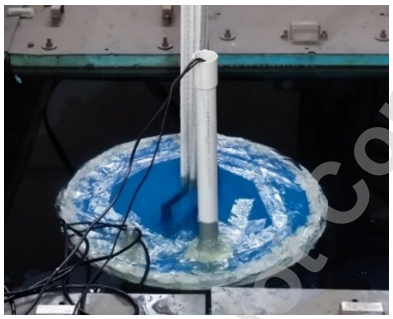

(b) Experimental set-up

(c) Method of hydrophone installation

Fig.6 Experimental test of underwater sound radiation

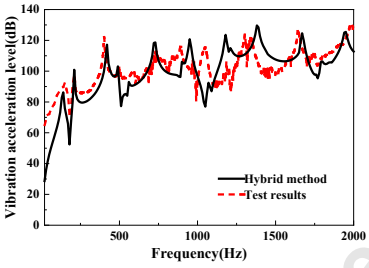

(a) The first test point

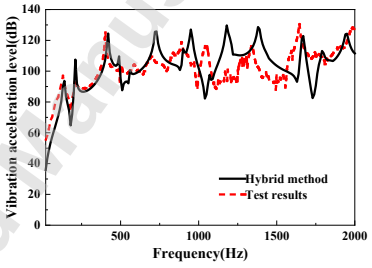

(b) The second test point

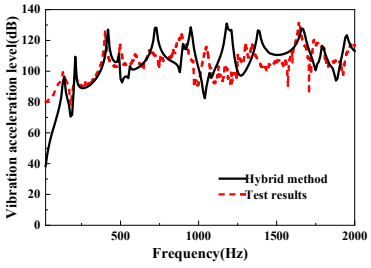

(c) The third test point

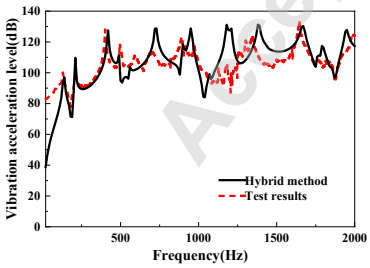

(d) The fourth test point

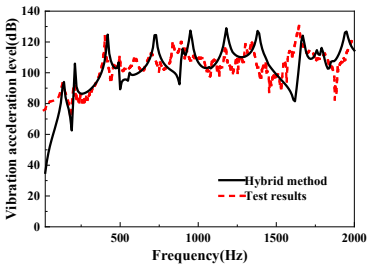

(e) The fifth test point

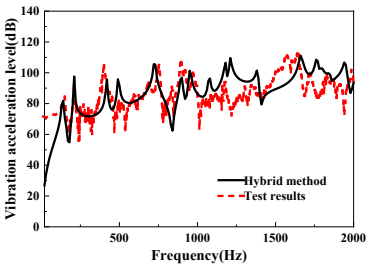

(f) The sixth test point

Journal of Vibration and Acoustics. Received October 29, 2023;
Accepted manuscript posted June 11, 2024. doi:10.1115/1.4065752

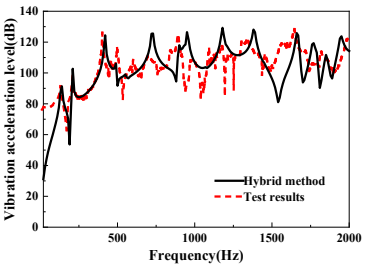

(g)The seventh test point

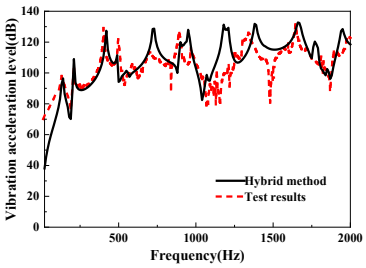

(h) The eighth test point

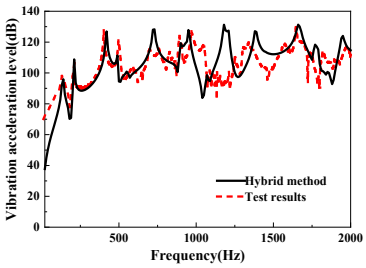

(i) The ninth test point

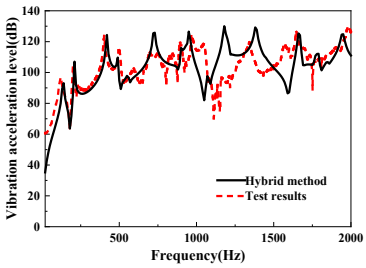

(j) The tenth test point

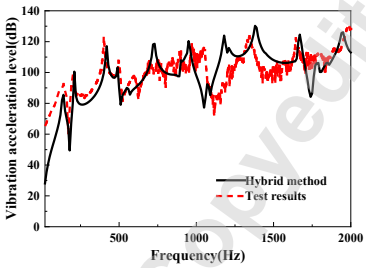

(k) The eleventh test point

Fig.7 The vibration response of the reference point

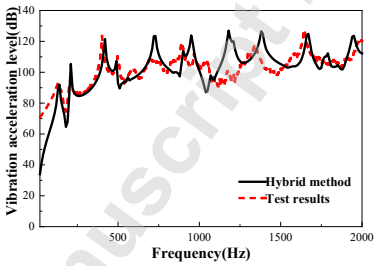

Fig.8 Mean vibration response of coupled structures

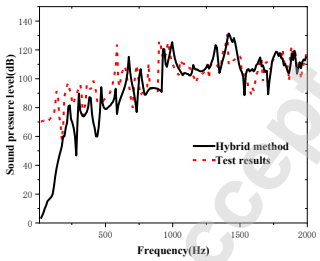

(a)Hydrophone 1

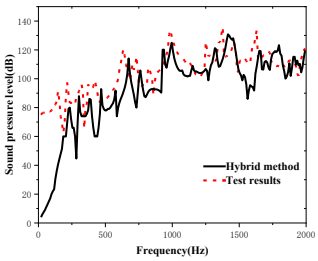

(b)Hydrophone 2

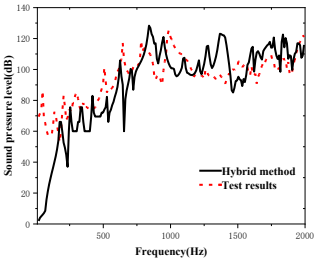

(c)Hydrophone 3

Fig.9 Sound pressure at the reference point

Journal of Vibration and Acoustics. Received October 29, 2023;
Accepted manuscript posted June 11, 2024. doi:10.1115/1.4065752

Table. 1 Comparison of natural frequency

Natural	Simulation	Experiment	inaccuracy
First-order	317	321	1.3%
Second-order	344	357	3.7%
Third-order	773	803	3.9%
Fourth-order	1318	1223	7.2%
Fifth-order	1691	1643	2.8%
Sixth-order	2003	2011	0.4%